High Capacity and Miniaturized Flexible Chipless RFID Tag Using Modified Complementary Split Ring Resonator

MOHD EZWAN B JALIL[1], MOHAMAD KAMAL A RAHIM[1], (Senior Member, IEEE), HIMDI MOHAMED[2], NOOR ASMAWATI BINTI SAMSURI[1], (Member, IEEE), NOOR ASNIZA MURAD[1], (Senior Member, IEEE), RAIMI DEWAN[3], (Member, IEEE), HUDA BIN A MAJID[4], (Member, IEEE), NUR BIHA MOHAMED NAFIS[1], LEVY OLIVIA NUR[5], (Member, IEEE), AND BAMBANG SETIA NUGROHO[5], (Member, IEEE)

[1]Advanced RF and Microwave Research Group, Faculty of Engineering, School of Electrical Engineering, Universiti Teknologi Malaysia, Johor 81310, Malaysia
[2]Institut d'Electronique et de Télécommunications de Rennes (IETR), UMR-CNRS 6164, Campus de Beaulieu, 35042 Rennes, France
[3]Advanced Diagnostics And Progressive Human Care (Diagnostic), Faculty of Engineering, School of Biomedical Engineering and Health Sciences, Universiti Teknologi Malaysia, Johor 81310, Malaysia
[4]Fakulti Teknologi Kejuruteraan (FTK), Universiti Tun Hussein Onn Malaysia, Hab Pendidikan Tinggi Pagoh, Johor 84600, Malaysia
[5]School of Electrical Engineering, Telkom University, Bandung 40257, Indonesia

Corresponding author: Mohamad Kamal A Rahim (mdkamal@utm.my)

ABSTRACT This paper aims to produce a high data capacity and miniaturized flexible chipless RFID tag based on the frequency signature using the Modified Complementary Split Ring Resonator (MCSRR). The proposed 19 bits chipless RFID tag using the frequency shifting technique consists of five slotted overlaying MCSRR with Different Width (MCSRR with DW) structures and the dimension of 48 mm × 48 mm. The structure is designed by using a flexible (Polyethylene Terephthalate) PET substrate with permittivity of 0.2. The operating frequency is between 0.9 GHz and 2.7 GHz. The advancement of slotted overlaying MCSRR with DW structures has successfully miniaturized the chipless RFID tag structure to about 107 mm^2/bit, $0.02\lambda_{mid}^2$/bit and 0.09 GHz/bit by maximizing the number of resonators in a limited space and minimizing the frequency separation between the resonators. The omnidirectional tag antenna is incorporated with the proposed MCSRR structure using the retransmission measurement method. The log-periodic antenna with a gain of 5-7 dBi is used for this measurement to improve the range distance between tag and reader system. Based on the retransmission measurement involving the antenna tag, the 19 bits chipless RFID tag which consists of five MCSRR with DW structures can be detected with a maximum range distance of 30 cm and a power transmitted level of 30 dBm.

INDEX TERMS Flexible chipless RFID tag, metamaterial, split ring resonator (SRR), retransmission method and size miniaturization.

I. INTRODUCTION

Chipless Radio Frequency Identification (RFID) is a wireless identification object that uses electromagnetic wave transmissions at specific regulated frequency bands. The technology is gaining more attention as it becomes a new alternative for short-distance communication to compete with existing RFID and optical barcodes. The chipless RFID successfully eliminates a computerized Applied Specific Integration Circuit (ASIC) microchip, which is usually the main component

The associate editor coordinating the review of this manuscript and approving it for publication was Chinmoy Saha.

of conventional RFID for storing memory information and is replaced with microwave element structures as the encoding elements [1]. The low-cost chipless RFID improves the identification applications in manufacturing, services, and product management, such as integration with the RF sensor, barcode replacement, and tracking positioning system. Furthermore, with the integration of the Internet of Things (IoT), the chipless RFID tag can execute the recognition task anywhere at any given time [2].

The chipless RFID system-based frequency signature uses the response of the transmission of electromagnetic signals for the identification of information detection.

The components of the chipless RFID consists of a reader system with transceiver antennas, multiple element microwave structure as an encoding element of chipless RFID and an antenna [3]. The chipless RFID tag contains a unique serial identification (ID) information from the multiple microwave element structure. The principle of a chipless RFID system begins by transmitting the interrogating signal to the chipless RFID tag using the high gain reader antenna. The chipless RFID tag with the ID information will respond to the RFID reader's signal using the retransmission and backscattering method [4]. Thus, choosing the right reader and tag antenna to maximize the range distance is essential. For the chipless RFID system, apart from producing good performance antenna and encoding elements, it is also crucial to choose materials that are flexible, compact and durable for all of the chipless RFID components, including the substrate and the conductive element [5]. Furthermore, the chipless RFID system mostly implements a frequency signature for encoding data due to its ability to maximize high capacity data with high range distance as compared to the time-domain signature [6].

The development of a chipless RFID tag using frequency signature with the backscattering and retransmission method has been getting much attention from the researchers as compared to the time domain technique due to its attractive properties such as having a higher maximum data capacity, a higher reading range and uses a simple system [7]. However, the capability of the chipless RFID tag is not sufficient to match the identification of barcode technology that can generate data capacity of up to 8-bit bytes. For the chipless RFID tag based frequency signature, the resonator number determines the chipless RFID's coding capacity. Typically, a single set of resonator represents 1-bit coding data [8], [9]. The addition of the number of resonators will improve the coding capacity of the chipless RFID tag. For example, two states (1-bit) resonator in a chipless RFID tag based on retro-radiator was designed with nine spiral filters separately as a coding element, producing 281 *mm/bit* and 0.23 *GHz/bit* [10]. The chipless RFID with a maximum capacity of 35 bits was provided with 35 spiral resonators with a size of 0.11 in λ^2_{middle}/bit [11]. Another author successfully achieved 3 bits per resonator using the micro strip resonator with a high ratio between frequency range and the bit, which is about 0.25 *GHz /bit* [6].

The main challenge of designing the chipless RFID based frequency signature is to enhance the coding capacity, which increases the structure size and requires a wide frequency range [12]. Thus, the issue needs to be addressed by minimizing the actual size of the chipless RFID structure per bit as shown in Equation (1) and the bandwidth allocation per bit as shown in Equation (2). The chipless RFID tag is required to utilize all provided frequency allocation to maximize high capacity data and to avoid interference with other signals. A miniaturized chipless RFID tag should use the entire resonator structure either on the ground plane or the substrate to maximize the resonator number. The miniaturized chipless

RFID tags will maximize the data capacity by providing high Q factors and narrowband resonators [13] accordingly.

Actual structure size per bit(λ^2_{mid}/bit)

$$= \frac{\text{Size}(\lambda^2) \text{ based middle operating frequency})}{\text{Number of bits}} \quad (1)$$

Bandwidth allocation per bit (GHz/bit)

$$= \frac{\text{Bandwidth (GHz)}}{\text{Number of bits}} \quad (2)$$

Most researchers have successfully developed the chipless RFID tags by using low loss and high-performance board materials such as the Duroid [14], Taconic [15], and Rogers boards [16]. However, these materials are rigid, expensive and not suitable to be placed on flexible objects. A flexible chipless RFID can maximize the potential for chipless RFID applications to any product with curved surfaces, such as boxes, papers, and plastic items [17]. However, most flexible materials have a high dielectric loss due to their thickness and loss tangent, thus disrupting the transmission signals for the detection process of the chipless RFID tag with ID information. Therefore, a feasibility study of the chipless RFID tag antenna and the encoding element with flexible material and high loss tangent should be well performed to ensure that the performance quality is still relevant to the chipless RFID detection process system.

A metamaterial is an artificial engineering material that exhibits unusual electromagnetic properties generally not found in nature. The artificial material with changing electromagnetic properties from positive to negative permittivity and permeability provides a potential solution to fulfill demand in designing modern microwave devices such as antenna [18], filter [19], lenses [20] and passive sensor [21]. It allows future researchers to improve their designs, making them smaller in size, exhibiting multiband behavior and better performance for the devices. The unique metamaterial properties of the SRR and CSRR have been implemented in the microwave design such as in antenna, filter, absorber, lens and coupler for size miniaturization [22], multiband behavior [23] and producing excellent performances[24]. The SRR and CSRR are small electrical resonators that originate from the coupling between the inner and the outer ring to create the first resonant frequency. Simultaneously, the increasing distributed capacitance and inductance between both rings have reduced the first resonant frequency. This condition is essential for size miniaturization.

In this work, a flexible, high data capacity and miniaturized chipless RFID tag system with an operating frequency range of 0.9-2.7 GHz was proposed. The proposed chipless RFID system consists of a chipless RFID tag based on metamaterial structures with a wideband tag antenna and a high gain reader antenna. The proposed 19 bits chipless RFID tag based frequency signature using five modified complementary split ring resonators with different width (MCSRR with DW) structure with a dimension of 48 mm × 48 mm was designed using flexible Polyethylene Terephthalate (PET) substrate with a permittivity of 2 and a loss tangent of 0.35.
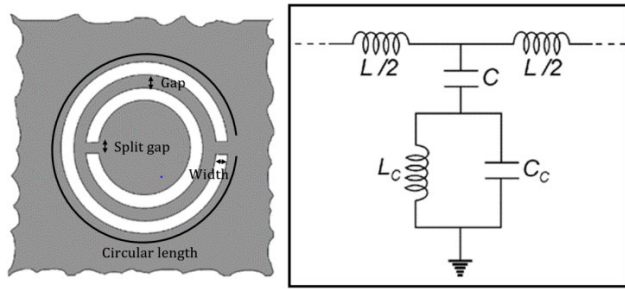
FIGURE 1. Equivalent circuit of CSRR with transmission line.

The advancement of slotted overlay MCSRR with DW structures has successfully improved the chipless RFID tag structure by optimizing the resonator number and minimizing the frequency separation distance between resonators. The compact egg-shaped monopole tag antenna with a slotted triangle ground plane was constructed using a flexible PET substrate which was incorporated with the proposed chipless RFID tag using MCSRR with DW structures for the retransmission method.

II. MINIATURIZED DESIGN USING CSRR STRUCTURE

Following the material selection, the miniaturized chipless RFID tag was designed on a flexible PET film material. The PET substrate was used as the main substrate element as it gives out the most optimum performance. The light-weight PET material has a moderate loss tangent of 0.35, producing optimum stop band resonator performances in terms of the deep and low resonant frequency.

Next, this research aims to discover the best design for the SRR metamaterial structure, including the size miniaturization and operating frequency range reduction. For a complementary split-ring resonator (CSRR), a negative image of the conventional split-ring resonator, an artificial metamaterial element is implemented as the primary design reference for the proposed chipless RFID tag design. This slotted ground plane resonator consists of a double C-shaped slot ring resonator in the opposite direction that behaves like a small LC resonant element circuit, as shown in Figure 1. The complementary split-ring resonator (CSRR) can provide a high-quality factor with strong electric coupling with an electromagnetic wave via a transmission line. Besides, the size dimension of the complementary split-ring resonator is smaller as compared to the resonant wavelength due to the additional capacitance and inductance on the element structure. A short circuit using $\lambda/2$ transmission line acts as a series of the resonator with high-quality factors. The semi lumped resonator, which is a small electrical resonant element, can be constructed by adding capacitance and inductance structures. These structures are introduced to reduce the size of the resonator. The resonant frequency of the semi lumped resonator equation is given by $f = 1/2\pi\sqrt{LC}$ where f is the frequency, L is the total inductance of the resonator and C is the total capacitance of the resonator.
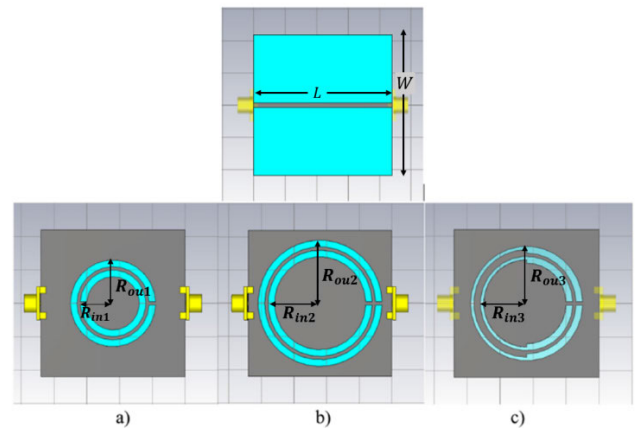

FIGURE 2. Proposed transmission line with resonator structure; a) CSRR structure, b) MCSRR structure c) MCSRR with DW structure with length, L = 44 mm, width, W = 44 mm, width of ring resonator = 2 mm, gap between resonator = 1 mm, split gap = 1 mm, radius of outer ring of CSRR, R_{ou1} = 13.00 mm, radius of inner ring of CSRR, R_{in1} = 10 mm, radius of outer ring of MCSRR, R_{ou2} = 19 mm, radius of inner ring of MCSRR, R_{in2} = 16 mm, radius of outer ring of MCSRR with DW, R_{ou3} = 17.00 mm and radius of inner ring of MCSRR with DW, R_{in3} = 14.00 mm.

In the miniaturized chipless RFID tag design, a transmission line with multiple narrowband slotted metamaterial resonators in the ground plane is employed to maximize the capacity of the identification coding element. The slotted metamaterial resonator structure generates the negative permittivity of material properties at a specific resonant frequency, affecting the base material performance and properties [25]. The investigation starts with the evaluation of three proposed SRR designs; primary complementary split ring resonator (CSRR), modified complementary split ring resonator (MCSRR) and the modified complementary split ring resonator with different width (MCSRR with DW) in terms of length size and the resonant frequency of outer and inner ring structures as shown in Figure 2. Firstly, a transmission line with resonators of CSRR structures using the PET substrate was simulated to study the variable effect of the resonant frequency and the electromagnetic field distribution on the CSRR structures for size miniaturization. The theoretical effective permittivity of a 50-ohm microstrip transmission line with CSRR structure is 1.71. Figure 2 shows all the parameter dimensions for the CSRR, MCSRR and MCSRR with DW structures.

A. SIZE COMPARISON FOR THE VARIATION OF THE MODIFIED CSRR

The specific designs presented in this section aim to achieve a miniaturized size for the tag according to the effective length of the resonators. Each resonator requires less effective wavelength λeff to obtain the smallest dimension possible. Next, the small frequency gap between the two resonating elements was determined to reduce the operating frequency. There are three types of slotted resonators with different structures; CSRR, MCSRR and MCSRR with DW. The slotted ground plane structures are connected with a transmission
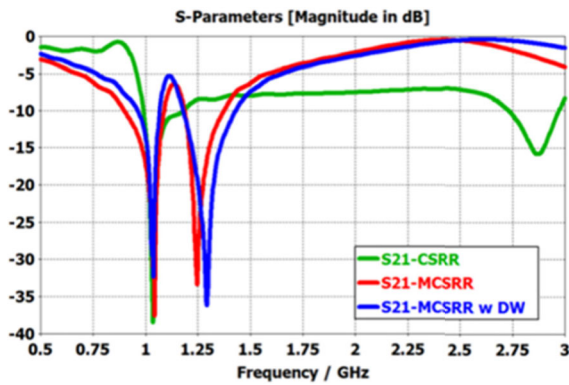
FIGURE 3. The simulated S_{21} insertion loss for the proposed design; CSRR (green), MCSRR (red), MCSRR with DW (blue).

TABLE 1. The simulated resonant frequency and bandwidth of S_{21} result for all of proposed metamaterial resonators.

Structure	First resonance (Bandwidth) (GHz)	Second resonance (Bandwidth)(GHz)
CSRR	1.03 (0.20)	2.87 (0.22)
MCSRR	1.04 (0.19)	1.25 (0.18)
MCSRR with DW	1.03 (0.10)	1.29 (0.25)

line between the two ports. The insertion loss between the two ports will encode information values depending on the resonant frequency position in the next section.

In designing a high-capacity data of chipless RFID, the single structure should maximize the resonator amount and have a small separation between resonant frequencies. The evolution of the MCSRR with DW from the CSRR structure aims to reduce the frequency gap between the two resonances and miniaturize the inner ring's size and the outer ring. For all designs, the first resonance is determined to be between 1.03-1.04 GHz, as shown in Figure 3. All parameters were fixed including the split gap, spacing between the rings and the width of rings.

Table 1 presents the simulated resonant frequency and the bandwidth of S_{21} result for all the proposed metamaterial resonators. From Table 2, the outer ring resonator of the CSRR structure with a circular length of 0.36λ, is about 50% smaller compared to the outer ring resonator of the MCSRR structure with a circular length of 0.54λ. However, the length of the inner ring resonator of CSRR with 0.77λ is about 69% larger than the inner ring resonator of the MCSRR structure with 0.54λ resonator as shown in Table 3.

Next, the operating frequency allocation depends on the range frequency between the two resonators. Increasing the number of resonators will increase the operating frequency range of the chipless RFID system. From the results, the MCSRR only required a frequency range of 7 % of the CSRR for two ring resonators. The MCSRR provides better performance for both ring size miniaturization and low gap frequency between the resonators.

The MCSRR with DW structure with length of $0.48-0.49\lambda$ for the inner and outer ring resonator was introduced by

TABLE 2. Dimension and the resonant frequency of first or outer ring resonator.

Structure	Circular Length (mm, λ)	Resonance frequency (GHz)
CSRR	80.69 , 0.36	1.03
MCSRR	118.40 , 0.54	1.04
MCSRR with DW	105.82 , 0.48	1.03

TABLE 3. Dimension and the resonant frequency of second or inner ring resonator.

Structure	Circular Length (mm, λ)	Resonance frequency (GHz)
CSRR	61.84, 0.77	2.87
MCSRR	99.54, 0.54	1.25
MCSRR with DW	86.98, 0.49	1.29

modifying the ring with two different widths for the left and right sides. The ring modification aims to miniaturize the actual size to about 11-13 % of the MCSRR structure with a circular length of 0.54 λ for the inner and outer rings. The MCSRR with DW structure was chosen as the best design among the proposed metamaterial structure for designing the chipless RFID tag. This is due to its miniaturized size and low gap frequency between the resonators.

B. SURFACE CURRENT DISTRIBUTION
The electromagnetic behavior of the metamaterial resonators can be studied by evaluating their surface current distribution at the simulation stage. The flow direction of the surface current will explain the metamaterial resonator's principal work at the resonant frequency. In this simulation research, the surface current was presented for each design of the metamaterial resonators; CSRR, MCSRR and MCSRR with DW. The simulated surface current distribution at the first resonant frequency for all metamaterial structures was analyzed in the $+ z$ direction on the *x-y* plane to understand how stopband works at the resonant frequency.

Figure 4 shows the surface current distribution for all slotted metamaterial structures at 1.03-1.04 GHz. The surface current at the strip or slotted gap between both ring flows in a different direction as compared to the external slotted outer ring. Strong surface current can be observed at the split gap of the outer ring for all metamaterial structures. The surface current shows that the resonant frequency depends on the inductance of the slotted gap and the capacitance of the slotted stub. The CSRR can produce small resonators due to its high capacitance and inductive between the inner and outer ring and the inductive split gap of the outer ring and gap. In contrast to the MCSRR and MCSRR with DW, the resonant frequency depends on the inductance split gap of the outer ring and the small gap. The resonant frequency is also dependant on the stub between the external inner ring and the internal outer ring

The surface current distribution at the second resonant frequency of all metamaterial structures, including the CSRR
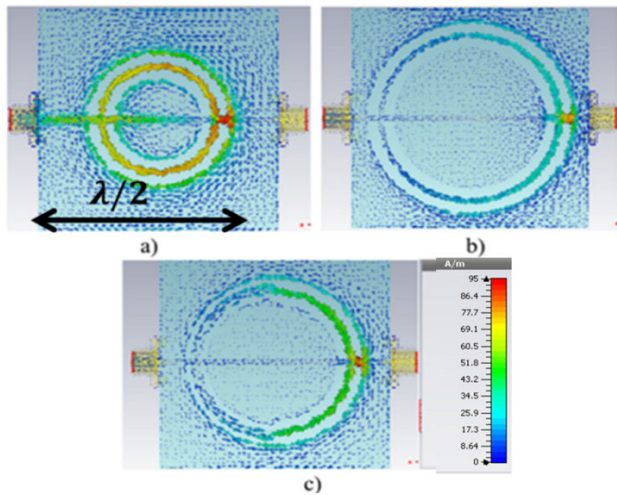
FIGURE 4. Surface current at the first resonant frequency for metamaterial structures; a) CSRR (1.03 GHz), b) MCSRR (1.04 GHz), c) MCSRR with DW (1.03 GHz).
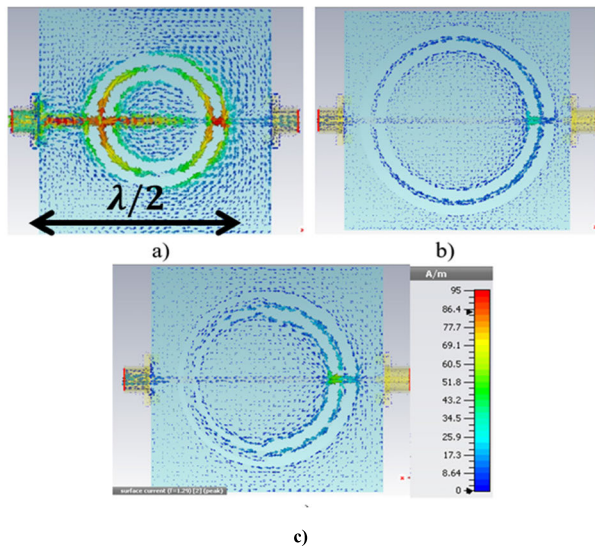

FIGURE 5. Surface current at the second resonant frequency for metamaterial structures; a) CSRR (2.87 GHz), b) MCSRR (1.25 GHz), c) MCSRR with DW (1.29 GHz).

structure at 2.87 GHz, MCSRR structure at 1.25 GHz and MCSRR with DW structure at 1.29 GHz were analyzed as shown in Figure 5. A strong current distribution can be observed at the split gap inner and outer ring for the CSRR structure. For MCSRR and MCSRR with DW structure, the current distribution is at 1.25 GHz and 1.29 GHz, respectively, with the split gap inner ring being the central radiating part of a resonator.

III. CSRR STRUCTURE AS ENCODING ELEMENT

This section discusses the parametric study of the split gap and the width of the inner ring and outer ring on S_{21} result. The parametric study was implemented into the miniaturized structure with low operating frequency; the slotted MCSRR with DW structure. The parametric study was to
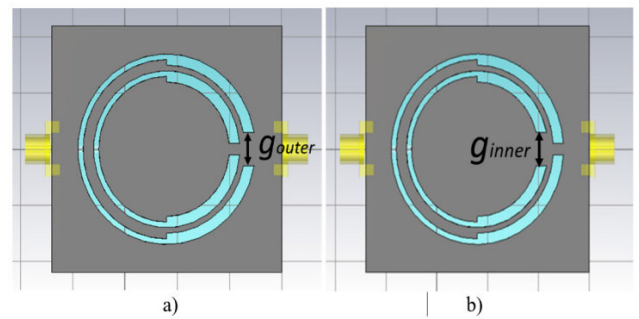
FIGURE 6. a) Varying split gap of outer ring b) Varying split gap of the inner ring.

identify the best sweeping parameter for the coding number of coding information using the frequency shifting technique. The parameter analysis was conducted using a time-domain solver with a mesh type of hexahedral Transmission Line Matrix (TLM) to balance between the accuracy and the simulation time. There are dominant parameters: split gaps that influence the resonant frequency based on the inductance and capacitance behaviors. During the parameter study, only one parameter was altered. In contrast, other parameters remain unchanged based on the previous dimension specification of the MCSRR with DW to clarify each parameter's effect on the performance of insertion. Then, the impact of each parameter on the transmission coefficient and resonant frequency was studied.

The circular ring length is the most predominant parameter of the circular ring in determining the resonant frequency of the MCSRR with DW resonator. In practice, increasing the circular length will reduce the resonant frequency of the MCSRR with DW resonator. In this section, the split gap inner ring and outer ring parameter on the transmission coefficient of MCSRR with DW are analyzed. The outer gap ring was varied from 2 mm to 6 mm with a step size of 1 mm, as shown in Figure 6.

Figure 7 shows that the high split gap of the outer ring value reduces the first resonant frequency and maintains the second resonant frequency between 1.29-1.30 GHz. The result shows that the resonating frequency is at 1.06 GHz, 1.09 GHz, 1.10GHz, 1.12 GHz and 1.13 GHz, when the split gap size is 2 mm, 3 mm, 4 mm, 5 mm and 6 mm respectively. Next, the inner ring gap is varied from 2 mm to 6 mm, as shown in Figure 8. The MCSRR with DW structure was simulated with a split gap of 2 mm, 3 mm, 4 mm, 5 mm and 6 mm and the second resonant frequency shows the value of 1.33 GHz, 1.36 GHz, 1.39 GHz, 1.41 GHz and 1.43 GHz respectively. The first resonance remains the same at 1.04 GHz despite a change in slipt gap.

A. RELATIONSHIP PARAMETER DIMENSION TO RESONANT FREQUENCY AND CIRCULAR RING LENGTH

Relationship parameter analysis aims to evaluate the linearity between the proposed parameters: the gap and width of the ring and the resonant frequency for the encoding process.
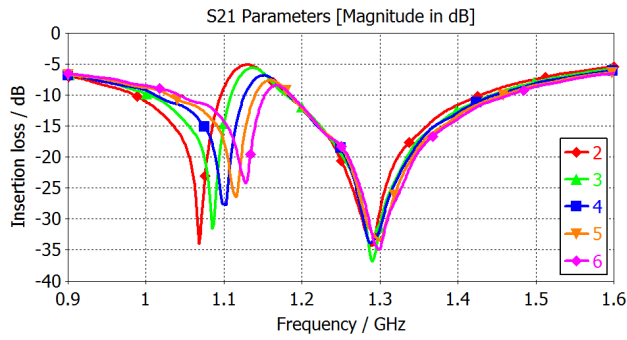
FIGURE 7. Simulated S_{21} insertion loss result with a varying split gap of the outer ring between 2 – 6 mm.
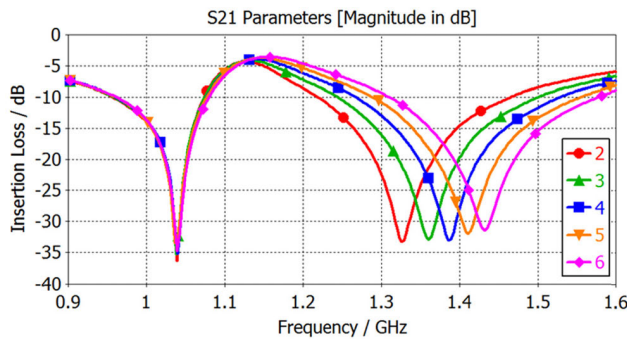

FIGURE 8. Simulated S_{21} insertion loss result with a varying split gap of the inner ring between 2 – 6 mm.

FIGURE 9. Relationship between the split gap of both rings parameter to resonant frequency and circular ring length.

A good correlation between the parameter dimension and the resonant frequency enables high accuracy with stable allocation for the maximized coding number of chipless RFID. Based on Figure 9, the split gap ring parameter significantly increases the circular ring length. When the split gap of the inner ring was varied from 2 to 6 mm, the first resonant frequency changed linearly from 1.33 to 1.44 GHz. When the split gap of the outer ring was varied from 2 to 6 mm, the second resonance changed linearly from 1.07 to 1.13 GHz. The high split gap parameter reduced the circular length of the ring while increasing the resonant frequency. The reducing inductance element of the circular ring with the split gap ring produced a lower circular length. The split gap between the rings is positively proportional to the resonant frequency and negatively proportional to the circular length.

IV. MINIATURIZED AND HIGH CAPACITY CHIPLESS RFID TAG DESIGN USING FLEXIBLE MATERIAL

This section shows the design of a high capacity, miniaturized and flexible chipless RFID tag based on the MCSRR with DW structure using the PET substrate. A similar method, by further extending the previous design, a chipless RFID tag based on the transmission line with five overlaying slotted MCSRR with different width (DW) structure was located below the PET substrate in Figure 10. Each ring resonator with a gap acts as a resonating element located on the middle ground plane. It can be seen, a 50 Ω transmission line with a width of 1.3 mm was placed at the top layer of the substrate.
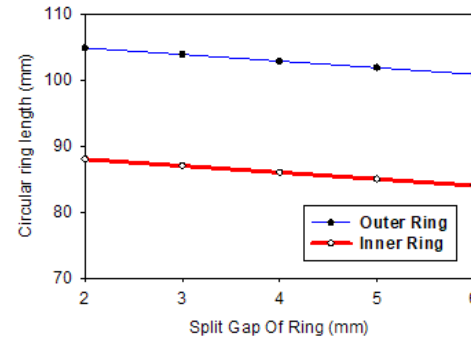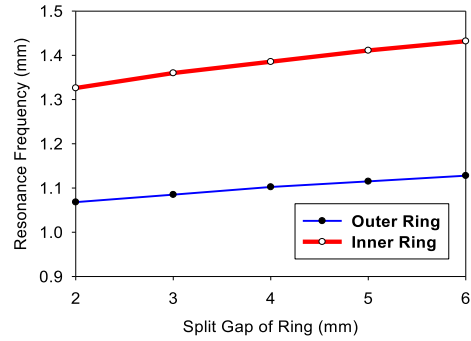
The overlaying slotted MCSRR with DW was implemented to improve size miniaturization by utilizing the ground plane's overall space and reducing the operating frequency by minimizing the two resonators' separating frequency. The adjustment of the MCSRR with DW structure will increase the capacitance and the inductance by reducing the slot width for the ring resonator's left side.

The fabricated prototype of the five modified complementary split-ring resonators with different width (MCSRR with DW) is shown in Figure 11. The dimension of the MCSRR is approximately $0.23\lambda_{low} \times 0.23\lambda_{low} \times 0.002\lambda_{low}$ where λ_{low} refers to the wavelength of the lowest resonant frequency of 1 GHz. The calculated circumference of all ring resonators with the split gap has a multiple of 0.48-0.49 λ resonant elements. The width of the resonating element w2, w3 and w4 were a fixed value of 1.8 mm. The other width, w5 and w1, which was 4.2 mm and 2.0 mm respectively, was aimed to reduce the resonant frequency of the 5th inner ring resonator to minimize frequency range. The split gap of each ring resonator parameter will be adjusted depending on the specific coding value of the chipless RFID tag.

As seen from Figure 12, the simulation and measurement of S_{21} results show valid agreement between each other. The simulated ideal resonant frequency performs well at 0.94 GHz, 1.10 GHz, 1.33 GHz, 1.68 GHz and 2.29 GHz, while the measured resonant frequency slightly shifts to 0.91 GHz, 1.07 GHz, 1.31 GHz, 1.66 GHz and 2.28 GHz. The measured result has no significant change than the simulated result due to the accurate determination of the substrate
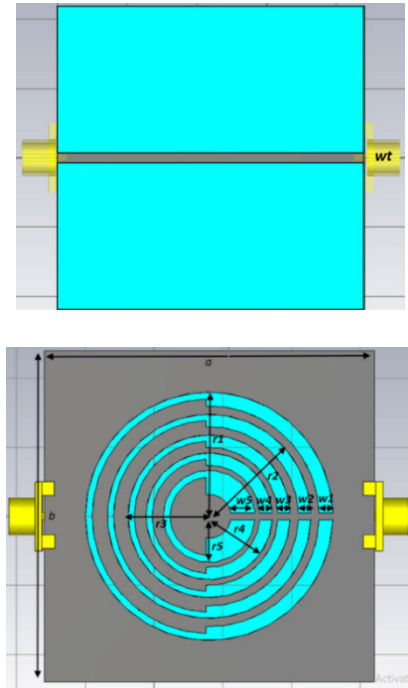
FIGURE 10. Final design of the chipless RFID tag for retransmission method a) front side and b) backside where width = 48 mm, length = 48 mm, height of substrate = 0.48 mm, r1 = 18.0 mm, r2 = 14.8 mm, r3 = 11.8 mm, r4 = 9.2 mm, r5 = 6.7 mm, w1 = 2.0 mm, w2 = 1.8 mm, w3 = 1.8 mm, w4 = 1.8 mm, w5 = 4.2 mm and wt = 1.3 mm.

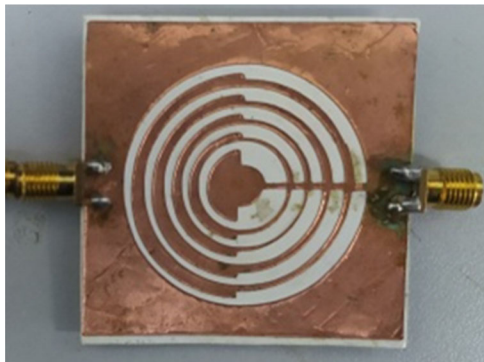**FIGURE 11.** Fabricated Prototype of the high capacity chipless RFID tag.

FIGURE 12. Simulation and measurement of transmission coefficient result for the chipless RFID tag.
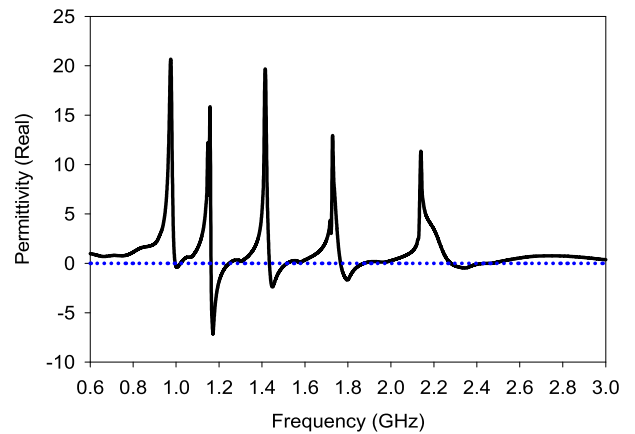
FIGURE 13. Effective permittivity from the S-parameter of prototype chipless RFID tag.

TABLE 4. The resonant frequency of each ring based on different split gap parameter.

Gap (No order)	First	Second	Third	Forth	Fifth
1.0 (1)	0.994	1.181	1.444	1.807	2.311
1.5 (2)	1.009	1.200	1.472	1.842	2.373
2.0(3)	1.020	1.216	1.495	1.877	2.434
2.5(4)	1.029	1.228	1.513	1.901	2.476
3.0(5)	1.036	1.239	1.528	1.926	2.525
3.5(6)	1.043	1.254	1.549	1.955	2.569
4.0(7)	1.047	1.256	1.556	1.968	2.581
4.5(8)	1.051	1.265	1.568	1.985	2.632
5.0(9)	1.059	1.273	1.582	2.012	2.681
5.5(10)	1.064	1.283	1.598	2.034	2.723
6.0(11)	1.071	1.294	1.614	2.054	-
6.5(12)	1.077	1.302	1.629	2.083	-
7.0(13)	1.081	1.309	1.642	2.096	-
7.5(14)	1.087	1.317	1.657	2.121	-
8.0(15)	1.094	1.326	1.671	2.141	-

permittivity of 2.0. However, the reduction of transmission coefficient level for the measured resonant frequency occurred due to a high substrate loss tangent of 0.35. Based on the design, the effective permittivity is extracted from the simulated S-parameter using the robust method [26]. The real permittivity curves reveal typical resonance properties. The negative permittivity will exist in frequency bands after the resonance frequencies as shown in Figure 13.

Table 4 shows the resonant frequency of all ring resonators, including the first, second, third, fourth and fifth rings by the various split gap of ring resonator parameters. The first, the second, the third, and the fourth rings have fifteen states, while the fifth ring has ten conditions based on the whole proposed operating frequency range. The operating frequencies for each resonator state are different from 0.99-1.09 GHz for the first ring, 1.18-1.33 GHz for the second
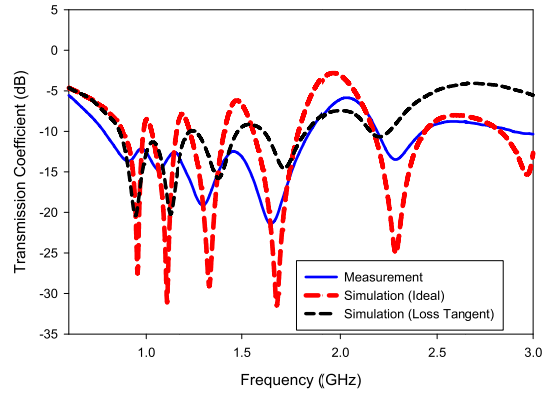
ring, 1.44-1.67 GHz for the third ring, 1.81-2.14 GHz for the fourth ring, and 2.31-2.72 GHz for the fifth ring.

The effect of the presence of high tangent loss reduces the sharpness of the resonance at specific frequencies. However, the coding process can be carried out with a minimum S_{21} value determination at the frequency range of each resonator. For example, if the first resonance frequency is 1,047 GHz in the frequency range between 0.994 and 1.094 GHz, then the
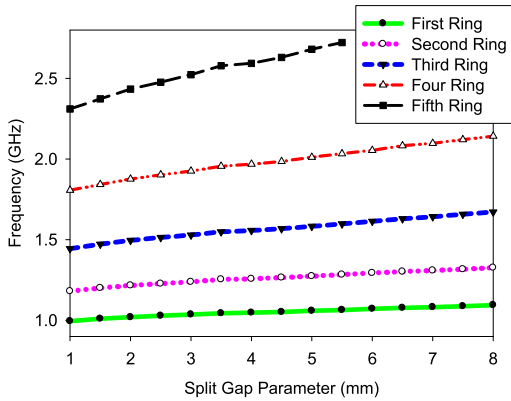
FIGURE 14. The relationship between split gap parameter and the resonance frequency.

FIGURE 15. The relationship between split gap parameter and the resonance frequency.

FIGURE 16. Simulated transmission coefficient of chipless RFID tag based multiple metamaterial resonator with different all split gaps.

FIGURE 17. Measured transmission coefficient of chipless RFID tag based multiple metamaterial resonator with a different all split gaps.

FIGURE 18. Chipless RFID tag structure with different ID code number a) 30 b) 450 c) 6750 d) 101 250 is shown as grey, red and blue line S_{21} result.

order number for the first resonator is 7. There is a frequency separation for each resonator to avoid overlapping in the same frequency range. For example, the separation allocation bandwidth between the first and the second resonator is 0.09 GHz and the second and third resonator is 0.12 GHz.

The relationship between the split gap parameter and the resonant frequency is shown in Figure 14. The identification code has five resonances in a specific order. The first, second, third, and fourth resonances have fifteen conditions. The fifth resonance has ten conditions. The correct number of permutation and ID information was determined based on the following calculation. Equation (3) was used to determine the ID code number for each chipless RFID tag.

$$P_1^{15} \times P_1^{15} \times P_1^{15} \times P_1^{15} \times P_1^{10}$$
$$= 15 \times 15 \times 15 \times 15 \times 10 = 506250 \text{ ID} \approx 19 \text{ bit}$$

ID code number
$$= ((No. order\ of\ condition\ for\ 1st\ ring - 1) \times 15^0)$$
$$+ ((No.\ order\ of\ condition\ for\ 2nd\ ring - 1)$$
$$\times 15^1) + ((No.\ order\ of\ condition\ for\ 3rd\ ring - 1) \times 15^2)$$
$$+ ((No.\ order\ of\ condition\ for\ 4th\ ring - 1) \times 15^3)$$
$$+ ((No.\ order\ of\ condition\ for\ 5th\ ring - 1 \times 15^4)) \quad (3)$$

The readings of the ID code number based on the different split gap parameter conditions of the chipless RFID tag using five MCSRR with DW structures is shown in Figure 15. Figure 16 shows the simulated normalized transmission coefficient with different split gaps for all resonators of the chipless RFID tag based metamaterial resonator. Each colour has a different split gap on each MCSRR which are 1mm for black, 3 mm for green and 4 mm for red. This condition allows the resonant frequency to be higher for each resonator due to the increase in the split gap in each resonator, which proved to be an effective result as it decreases the size of each resonator. According to Figure 17, the trend of the measured results gave good agreement with the simulated results with a slight difference in the resonant frequency.

The split gap of the single resonator of the chipless RFID tags was changed to 2 mm to investigate the effect of changing the split gap of a single resonator on other resonant frequency
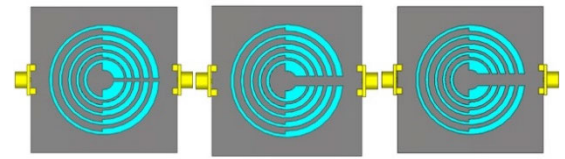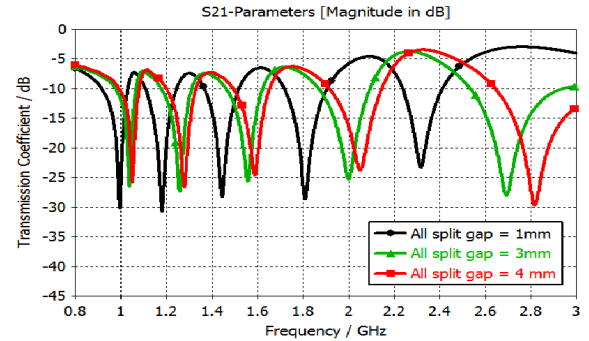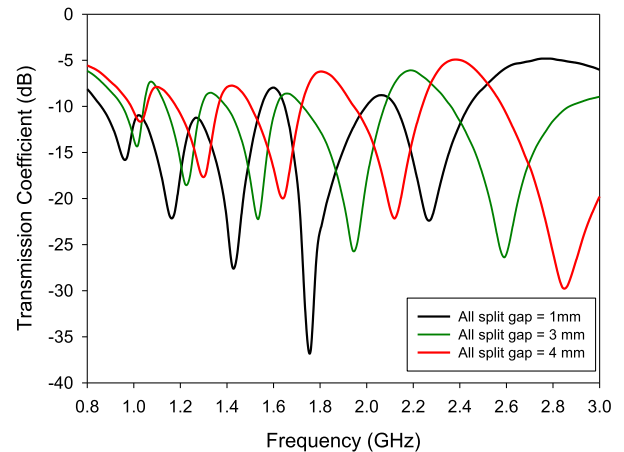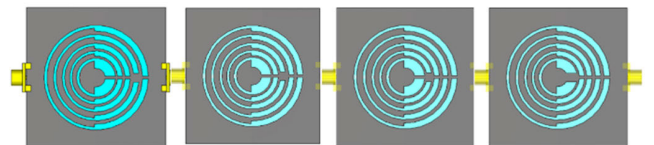
of resonators as shown in Figure 18. Other split gap resonators were fixed to 1 mm. However, the second split gap for brown, the third split gap for red, the fourth split gap for blue, and the fifth split gap for green were changed to 2 mm. Based on Figure 19 the change in the individual value of the split gap resonator does not modify the resonant frequency for other resonators. Figure 20 exhibits that the measured result has a strong trend with the simulated results.
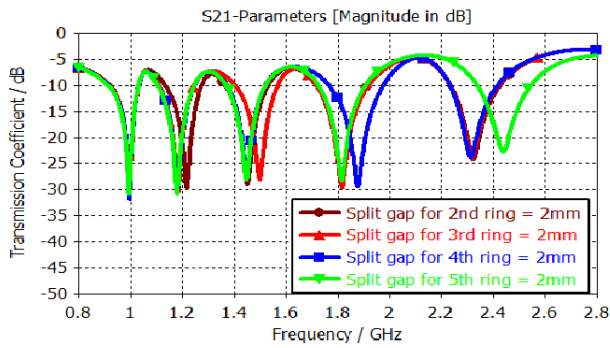
FIGURE 19. Simulated transmission coefficient of chipless RFID tag based multiple metamaterial resonator with 2 mm split gap on different rings.
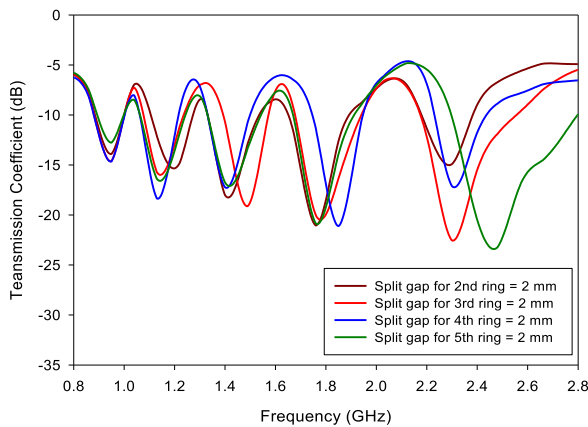

FIGURE 20. Measured transmission coefficient of chipless RFID tag based multiple metamaterial resonator with 2 mm split gap on different rings.
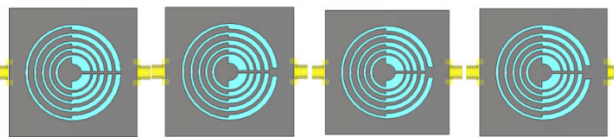

FIGURE 21. Chipless RFID tag structure for blue, green, black and grey line S_{21} result.

The split gap on the first resonator ring was changed to 1 mm, 3 mm, 4 mm, and 5 mm as shown in Figure 21. This was conducted to study the effect of shifting low-frequency resonance towards the resonant frequency of other resonators. Typically, changes in low frequency will change the other resonant frequencies due to the coupling effect between the elements. According to Figure 22, the simulation results show that the resonant frequency of the resonator increased with the split gap. No change occurred in the other resonators when the first split gap resonator was changed. The simulation results from Figure 22 and measured results from Figure 23 show a good agreement with each other. However, slight changes were made to the other resonators, with a difference of 0.01 GHz in the second ring, 0.01 GHz in the third ring, 0.04 GHz in the fourth ring, and 0.06 GHz in the fifth ring due to the manual fabrication factor of the attached two surfaces of the chipless RFID tags.
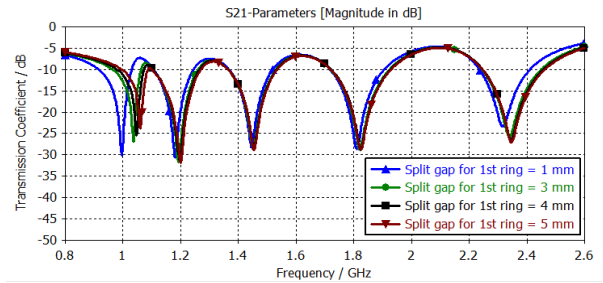

FIGURE 22. Simulated transmission coefficient of chipless RFID tag based multiple metamaterial resonator with the different split gap on first rings.
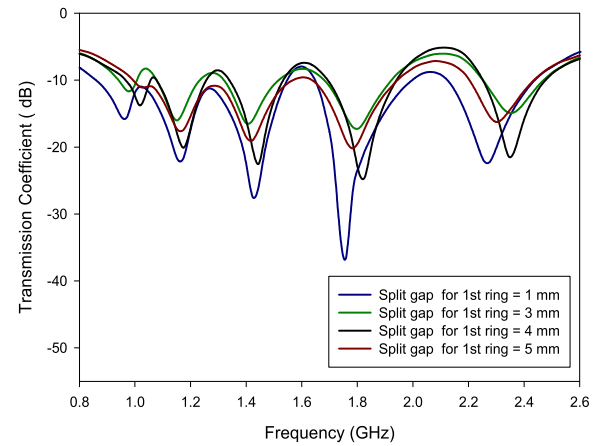

FIGURE 23. Measured transmission coefficient of chipless RFID tag based multiple metamaterial resonator with different split gap on first rings.

V. CHIPLESS RFID MEASUREMENT AND RESULT USING RETRANSMISSION METHOD

The compact and wide egg-shaped monopole antenna with a slotted triangle-shaped ground plane tag antenna was designed, simulated and fabricated with a dimension of 40 mm × 120 mm using PET substrate as shown in Figure 24, operating between 0.9 GHz and 2.9 GHz. The $0.17\lambda_{low} \times 0.51\lambda_{low}$ omnidirectional monopole antenna improved the overall bandwidth and the gain antenna compared to the conventional circular monopole antenna. The ground plane was adjusted by changing from a square to a triangular structure to improve the high frequency band at 2.9 GHz. Based on the result, the monopole antenna provides a doughnut shape and an omnidirectional radiation pattern. Based on Figure 25, the simulation and fabrication of S_{11} results are valid with a slight difference. Turning to a polar plot as shown in Figure 26, the E-plane pattern is similar to the eight-shaped pattern, while the H-plane pattern provides a circular shape.

The chipless RFID tag based retransmission method was designed using the flexible PET substrate. Incorporation between two proposed omnidirectional wideband egg-shaped monopole tag antenna with slotted triangular ground plane and the metamaterial resonator consists of five MCSRR with DW structures as the encoding elements produced the chipless RFID tag as shown in Figure 27. The monopole wideband antennas operating between 1 GHz and 3 GHz were
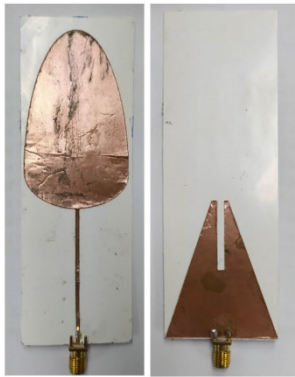
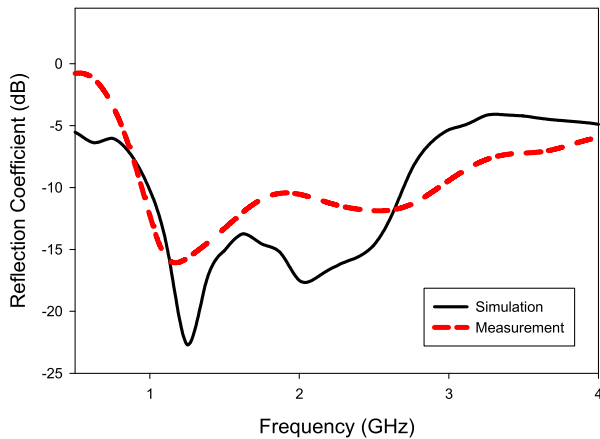**FIGURE 24.** Fabricated the egg-shaped monopole tag antenna.

FIGURE 25. Simulated and measured S_{11} result of the monopole antenna with a slotted triangle-shaped ground plane operating between 0.9-2.7 GHz.
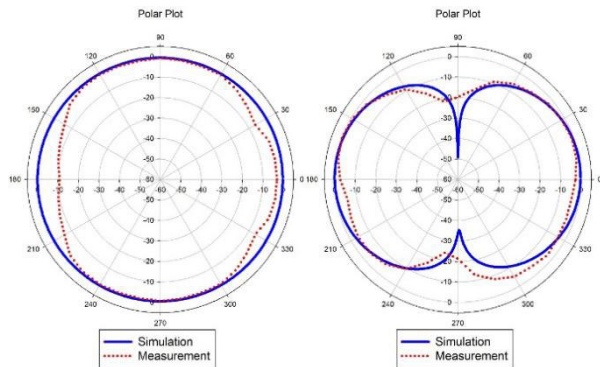

FIGURE 26. Simulated and measured radiation pattern of egg-shaped monopole tag antenna at 1.5 GHz.

connected to both ends of the multiple MCSRR structures with different polarization orientation to reduce mutual coupling between both reader antennas as shown in Figure 27. In terms of the design, the 50-ohm transmission line passes through the center of the split gap of the metamaterial resonator located on the ground plane. The L-shaped chipless RFID tag based retransmission has a substrate area of 112 cm². The proposed encoding element of the chipless RFID tag with 0 ID number using MCSRR with DW structures, all with different split gaps of 1 which was discussed
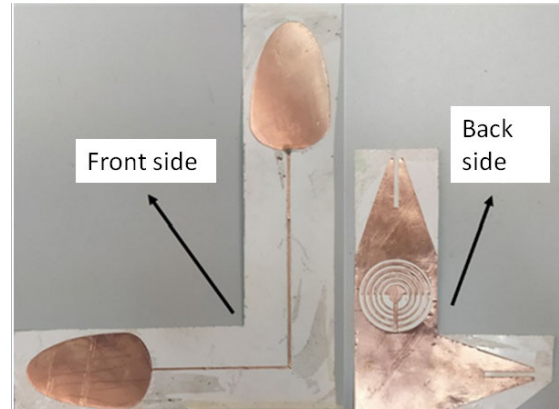

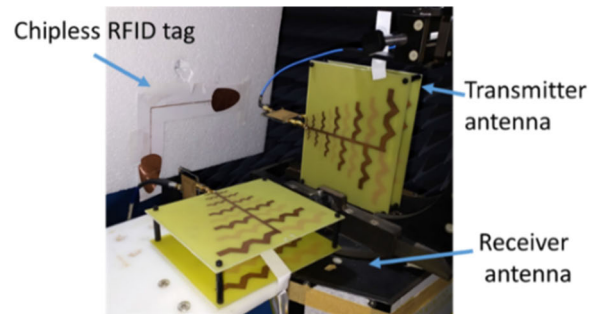**FIGURE 27.** Fabricated chipless RFID tag for retransmission method.

FIGURE 28. Measurement setup for proposed chipless RFID tag with the reader antenna for retransmission method.

previously, was used to test for all the chipless RFID based retransmission measurement.

The experimental measurement was done in the anechoic chamber to ensure the detection of the chipless RFID tag based retransmission method without external signal interruption and noise effect. The measurement setup consists of a pair of the double elements of the miniaturized Log-Periodic Second Series Koch Dipole Array (LPSKKDA) antenna as the transmitter and the receiver of the chipless RFID reader system and network analyzer with output power level between the ranges of -15 to 0 dBi for transmission coefficient measurement as shown in Figure 28. The pair with a gain of 6.8-7.5 dBi double element of LPSKKDA as the reader antenna were placed at a different orientation to ensure different polarization to minimize the cross-talk between antennas. The external amplifier with a gain of 30 dB in the range between 1- 3 GHz boosted the input power transmitted to improve the transmission coefficient performance level. The chipless RFID tag including the resonator and the tag antenna was attached to the low loss foam with permittivity of 1 and thickness of 2.5 cm. All S_{21} measurements of the chipless RFID tag were normalized to the chipless RFID tag without a resonator to simplify the detection chipless RFID tag process.

For the passive chipless RFID tag system-based retransmission method, the reading detection capability depends on the amount of power transmitted to the input value. Generally, the chipless RFID tag-based retransmission method will only send a weak signal back with a minimum distance range to the
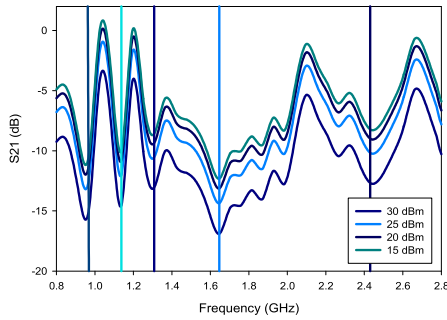
FIGURE 29. Measured normalized S_{21} result for the proposed chipless RFID tag for the retransmission method with power transmitted input.
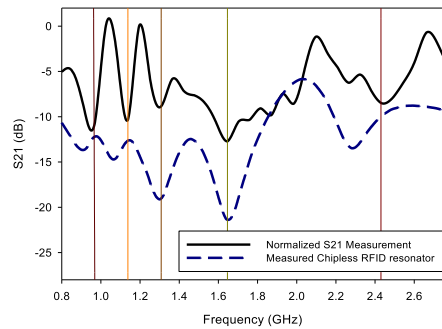

FIGURE 30. Measured normalized S_{21} result for the proposed chipless RFID tag for the retransmission method with a distance of 15 cm.

FIGURE 31. Measured normalized S_{21} result for the proposed chipless RFID tag for the retransmission method with a distance of 30 cm.

transmitter, especially small tag sizes with an omnidirectional antenna. Therefore, sufficient power transmission is required to ensure that the chipless RFID tags based on the retransmission method can be detected, mainly the resonant frequency of stopband providing ID code information.

In this experiment, the power transmitted to the input was determined by a network analyzer. The fixed power amplifier with a gain of 30 dB adjusted the overall amount of power transmitted, which is between the values of 30 dBm and 15 dBm. The chipless RFID was placed 15 cm from the log-periodic reader antennas. Based on Figure 29, all four readings can be read well with a slight difference in the transmission coefficient level between 0 to −15 dB. The normalized S_{21} values of the chipless RFID tags measurement-based retransmission method was conducted at two different distances, which were 15 cm, as shown in Figure 30, and 30 cm as shown in Figure 31. These distances were measured between the chipless RFID tag and the reader antenna. Both normalized S_{21} results were compared and evaluated with the measured metamaterial chipless RFID resonator The measured normalized S_{21} of chipless RFID and measured chipless RFID resonator have a valid and acceptable trend. However, the resonant frequency of the normalized S_{21} result at all stopband slightly changed when compared to the measured chipless RFID resonator due to misalignment during the setup, fabrication inaccuracy with hand and machine, and limited performance of network analyzer.

For measured normalized S_{21} with a range distance of 15 cm, the stopband frequency resonates at 0.95 GHz,
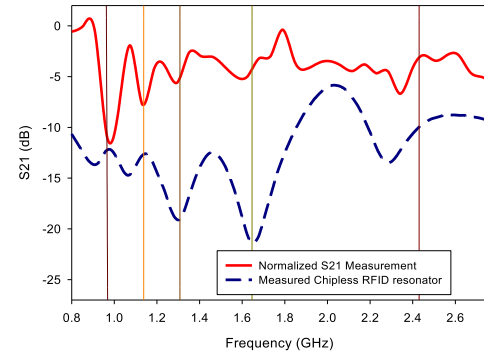
1.14 GHz, 1.30 GHz, 1.64 GHz and 2.44 GHz. For the range distance of 30 cm, the normalized S_{21} results of the chipless RFID tag were not significantly different as compared to the range distance of 15 cm. The work shows that the stopband frequency performs well at 0.98 GHz, 1.13 GHz, 1.29 GHz, 1.60 GHz and 2.35 GHz. The average normalized S_{21} level of all stopbands for 15 cm, which is about −10 dB, has a better performance than with the range distance of 30 cm which is about −7.3 dB. The high distance and high frequency will disrupt the performance of the chipless RFID tag measurement with free space path loss.

Table 5 shows the comparison of different types of chipless RFID based frequency signature. Some designs have been reported to reach more than 1 bit/resonator and less than 1 in λ^2/bit. According to Table 5, the highest bit for a single resonator is a 30 bit chipless RFID tag based C-shaped open-end resonator with 6 bits per resonator.

Furthermore, the smallest size of the chipless RFID tag per amount number of bit resonator is determined based on the area dimension of the chipless RFID tag in lambda of the center operating frequency per bit, λ^2/bit. The parameter of λ^2/bit is aimed to determine the miniaturized chipless RFID sizes by standardizing all the parameters such as the relative permittivity and frequency range. The smallest miniaturized chip RFID was successfully produced using the 23-bit metallic strip resonator with a λ^2/bit of 0.02. Besides that, the chipless RFID using the lowest frequency range per bit resonator is a 20-bit dipole array-plate with a frequency range per bit, GHz/bit of 0.07. The average frequency range per bit resonator, GHz/bit for all designs in the table is 0.27 GHz/bit. The proposed design managed to reach an actual size as low as $0.007\lambda^2$/bit by maximizing bits/resonator by 3.8 using frequency shifting technique. The integration between the tag antenna and the proposed design for range distance improvement makes the actual size increase from 0.007 to 0.040 λ^2/bit.

Figure 32 shows the overall process for the chipless RFID measurement using the retransmission method in the form of a flowchart including the S_{21} normalization procedure. The chipless RFID tag consists of a metamaterial resonator combination as an encoding element and a pair of tag antennas. The reader antennas are separated between each other

TABLE 5. Comparison of the proposed chipless RFID tag based transmission line and backscattering method.

| Chipless RFID Types	ε_r	Number of bits	Bit/ resonator	mm²/ bit	λ_{mid}^2 /bit	Frequency range (GHz)	GHz/bit	Tag Antenna
Spiral Resonator [11]	2.5	35	1	163	0.11	3-7	0.11	Yes
C-shaped open end [27]	3.5	30	1	21	0.04	3-11	0.26	No
Metallic Strip Resonator [28]	4.4	23	4.6	35	0.02	2-7	0.21	No
Dipole Array-Plate [29]	3.7	20	1	189	0.03	2.2-3.6	0.07	No
Cross- Dipole [30]	10.7	20	4	101	0.17	2-5	0.15	No
Nested Square Loop [31]	2.6	18	3	10	0.04	8-14	0.33	No
Dual-polarized Slot [32]	2.5	16	1	16	0.04	6-13	0.44	No
Quasi-complementary [33]	4.4	16	1	36	0.04	2-7	0.31	No
Antenna Open stub [34]	3.4	16	1	412	0.66	4-9	0.31	Yes
Spiral – Retro-radiator [10]	3.5	10	1	281	0.36	4.7-7	0.23	Yes
Coplanar waveguide[35]	3.7	8	1	1059	0.88	3-6	0.38	Yes
Open Stub Resonator [36]	4.4	8	1	600	0.26	1.5-4.5	0.38	Yes
Proposed design	**2.0**	**19**	**3.8**	**106**	**0.007**	**0.9-2.7**	**0.09**	**No**
Proposed design with the tag antenna	**2.0**	**19**	**3.8**	**589**	**0.04**	**0.9-2.7**	**0.09**	**Yes**
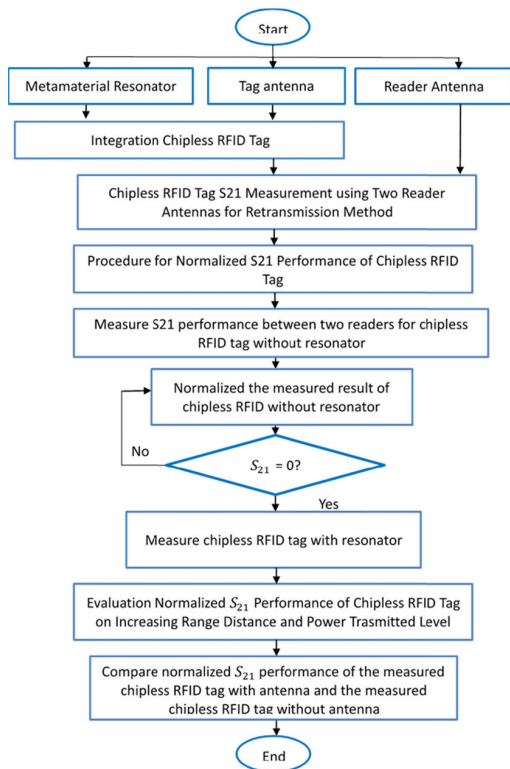
FIGURE 32. The flowchart for the chipless RFID system using the retransmission technique.

at about 10 cm. The normalized S_{21} value of both reader antennas with different polarization was measured with the proposed chipless RFID tag. The distance range between the chipless RFID tag and reader system was set between 15 and 30 cm and the power transmitted was set between 0-30 dBm by controlling the power input source from the network analyzer and external amplifier.

For the retransmission method, the chipless RFID tag consists of separating elements of the encoding element and two tag antennas with different polarization. The receiving end of the tag antenna will receive a signal from the antenna reader to carry through a multi-resonant element acting as code information for the chipless RFID. Then, the interrogation signal is transmitted back to the antenna reader using a transmitter of tag antenna with different polarization.

VI. CONCLUSION
Flexible, high data capacity and miniaturized chipless RFID tag based CSRR metamaterial structure with a minimized frequency operation was introduced in this paper. The potential 19 bits chipless RFID tag-based frequency signature using 5 overlaying of MCSRR with DW structures with dimensions of 48 mm ×48 mm ($0.38\lambda_{mid} \times 0.38\lambda_{mid}$), was successfully designed by using the flexible PET substrate with a permittivity of 2 and a loss tangent of 0.35, which operated between 0.9 GHz to 2.7 GHz. The multiple elements of the slotted MCSRR overlapped each other to minimize the proposed chipless RFID with full utilization of the ground plane space. The transmission line with multiple MCSRRs acted as the encoding element with 506 250 ID information using the frequency shifting technique to maximize data capacity. Then, the chipless RFID tag structure was improved by developing MCSRR with different widths (DW) to maximize the number

of resonators for each structure and minimize the frequency separation between resonators.

Furthermore, the development of the chipless RFID system was conducted to optimize the range distance between the reader system and the chipless RFID tag. The compact and wideband egg-shaped monopole tag antenna with a slotted triangle antenna was fabricated using a flexible PET substrate operating from 0.90 GHz - 2.75 GHz. The omnidirectional tag of the antenna was easily incorporated with the proposed encoding element with the MCSRR structure for the retransmission measurement method.

Finally, the evaluation of the performance of the proposed chipless RFID system was conducted using the retransmission and backscattering method to compare and evaluate the maximum distance range of the chipless RFID system. Based on the retransmission method involving the antenna tag used, the chipless RFID tag consisting of 5 MCSRR can only be detected at a maximum range distance of 30 cm with a power transmitted level of 30 dBm.

REFERENCES
[1] T. Athauda and N. Karmakar, "Chipped versus chipless RF identification: A comprehensive review," *IEEE Microw. Mag.*, vol. 2, no. 9, pp. 47–57, Sep. 2019.

[2] J. Aliasgari, M. Forouzandeh, and N. Karmakar, "Chipless RFID readers for frequency-coded tags: Time-domain or frequency-domain?" *IEEE J. Radio Freq. Identificat.*, vol. 4, no. 2, pp. 146–158, Jun. 2020.

[3] S. Preradovic, S. M. Roy, and N. C. Karmakar, "RFID system based on fully printable chipless tag for paper-/plastic-ltem tagging," *IEEE Antennas Propag. Mag.*, vol. 53, no. 5, pp. 15–32, Oct. 2011.

[4] F. Babaeian and N. C. Karmakar, "Development of cross-polar orientation-insensitive chipless RFID tags," *IEEE Trans. Antennas Propag.*, vol. 68, no. 7, pp. 5159–5170, Jul. 2020.

[5] M. U. A. Khan, R. Raad, J. Foroughi, F. Tubbal, P. I. Theoharis, and M. S. Raheel, "Effects of bending bow-tie chipless RFID tag for different polymer substrates," in *Proc. 13th Int. Conf. Signal Process. Commun. Syst. (ICSPCS)*, Dec. 2019, pp. 1–4.

[6] W. M. Abdulkawi and A.-F. A. Sheta, "K-state resonators for high-coding-capacity chipless RFID applications," *IEEE Access*, vol. 7, pp. 185868–185878, 2019.

[7] B. Aslam, K. U. Hasan, A. Habib, Y. Amin, and H. Tenhunen, "Frequency signature chipless RFID tag with enhanced data capacity," *IEICE Electron. Exp.*, vol. 12, no. 17, pp. 1–6, Sep. 2015.

[8] P. Prabavathi and S. S. Rani, "Design of frequency-signature based multiresonators using quarter wavelength open ended stub for chipless RFID tag," in *Proc. 25th Nat. Conf. Commun. (NCC)*, Feb. 2019, pp. 1–6.

[9] M. E. Jalil, M. K. A. Rahim, N. A. Samsuri, and R. Dewan, "Chipless RFID tag based on meandered line resonator," in *Proc. IEEE Asia–Pacific Conf. Appl. Electromagn. (APACE)*, Dec. 2015, pp. 203–206.

[10] H. Li, B. Wang, M. Wu, J. Zhu, and C. Zhou, "Design and analysis of chipless RFID tags based on retro-radiators," *IEEE Access*, vol. 7, pp. 148208–148217, 2019.

[11] S. Preradovic, I. Balbin, N. C. Karmakar, and G. F. Swiegers, "Multiresonator-based chipless RFID system for low-cost item tracking," *IEEE Trans. Microw. Theory Techn.*, vol. 57, no. 5, pp. 1411–1419, May 2009.

[12] F. Babaeian and N. C. Karmakar, "Compact multi-band chipless RFID resonators for identification and authentication applications," *Electron. Lett.*, vol. 56, pp. 9–11, May 2020.

[13] L. Wang, T. Liu, J. Sidén, and G. Wang, "Design of chipless RFID tag by using miniaturized open-loop resonators," *IEEE Trans. Antennas Propag.*, vol. 66, no. 2, pp. 618–626, Feb. 2018.

[14] W. M. Abdulkawi and A.-F.-A. Sheta, "Four-state coupled-line resonator for chipless RFID tags application," *Electronics*, vol. 8, no. 5, p. 581, May 2019.

[15] S. Preradovic and N. C. Karmakar, "Multiresonator based chipless RFID tag and dedicated RFID reader," *IEEE MTT-S Int. Microw. Symp. Dig.*, May 2010, pp. 1520–1523.

[16] I. Jabeen, A. Ejaz, A. Akram, Y. Amin, and H. Tenhunen, "Miniaturized slot chipless RFID tag for IoT applications," in *Proc. Int. Symp. Recent Adv. Electr. Eng. (RAEE)*, Aug. 2019, pp. 1–4.

[17] Z. Li and S. Bhadra, "A flexible printed chipless RFID tag for concentration measurements of liquid solutions," in *Proc. IEEE SENSORS*, Oct. 2019, pp. 1–4.

[18] J. Zhang, S. Yan, and G. A. E. Vandenbosch, "Metamaterial-inspired dual-band frequency-reconfigurable antenna with pattern diversity," *Electron. Lett.*, vol. 55, no. 10, pp. 573–574, May 2019.

[19] C. Tan, Y. Wang, Z. Yan, X. Nie, Y. He, and W. Chen, "Superconducting filter based on split-ring resonator structures," *IEEE Trans. Appl. Supercond.*, vol. 29, no. 4, pp. 1–4, Jun. 2019.

[20] B. Orazbayev, V. Pacheco-Pena, M. Beruete, and M. Navarro-Cia, "A self-supporting broadband zoned fishnet metamaterial lens operating at the millimeter-wave V-band," in *Proc. 9th Int. Congr. Adv. Electromagn. Mater. Microw. Opt. (METAMATERIALS)*, 2015, pp. 241–243.

[21] L. Dong, L. F. Wang, and Q. A. Huang, "Enhancing the readout of passive wireless sensors by using left-handed metamaterials," in *Proc. IEEE Sensors*, Oct. 2017, pp. 1–3.

[22] M. Ramzan and K. Topalli, "A miniaturized patch antenna by using a CSRR loading plane," *Int. J. Antennas Propag.*, vol. 2015, pp. 1–9, Jul. 2015.

[23] P. M. Paul, K. Kandasamy, and M. S. Sharawi, "A triband circularly polarized strip and SRR-loaded slot antenna," *IEEE Trans. Antennas Propag.*, vol. 66, no. 10, pp. 5569–5573, Oct. 2018.

[24] L. Peng, S. Sang, Z. Wang, H. Jin, A. Wu, K. Xu, and G. Wang, "Wideband radiation from an offset-fed split ring resonator with multi-order resonances," *IEEE Antennas Wireless Propag. Lett.*, vol. 17, no. 12, pp. 2198–2202, Dec. 2018.

[25] F. Falcone, T. Lopetegi, J. D. Baena, R. Marques, F. Martin, and M. Sorolla, "Effective negative-ε stopband microstrip lines based on complementary split ring resonators," *IEEE Microw. Wireless Compon. Lett.*, vol. 14, no. 6, pp. 280–282, Jun. 2004.

[26] X. Chen, T. M. Grzegorczyk, B.-I. Wu, J. Pacheco, and J. A. Kong, "Robust method to retrieve the constitutive effective parameters of metamaterials," *Phys. Rev. E, Stat. Phys. Plasmas Fluids Relat. Interdiscip. Top.*, vol. 70, no. 1, Jul. 2004, Art. no. 016608.

[27] T. Noor, A. Habib, Y. Amin, J. Loo, and H. Tenhunen, "High-density chipless RFID tag for temperature sensing," *Electron. Lett.*, vol. 52, no. 8, pp. 620–622, Apr. 2016.

[28] A. Vena, E. Perret, and S. Tedjini, "Chipless RFID tag using hybrid coding technique," *IEEE Trans. Microw. Theory Techn.*, vol. 59, no. 12, pp. 3356–3364, Dec. 2011.

[29] M. Svanda, M. Polivka, J. Havlicek, J. Machac, and D. H. Werner, "Platform tolerant, high encoding capacity dipole array-plate chipless RFID tags," *IEEE Access*, vol. 7, pp. 138707–138720, 2019.

[30] M. Khaliel, A. El-Awamry, A. F. Megahed, and T. Kaiser, "A novel design approach for co/cross-polarizing chipless RFID tags of high coding capacity," *IEEE J. Radio Freq. Identificat.*, vol. 1, no. 2, pp. 135–143, Jun. 2017.

[31] H.-F. Huang and L. Su, "A compact dual-polarized chipless RFID tag by using nested concentric square loops," *IEEE Antennas Wireless Propag. Lett.*, vol. 16, pp. 1036–1039, 2017.

[32] M. A. Islam and N. C. Karmakar, "A novel compact printable dual-polarized chipless RFID system," *IEEE Trans. Microw. Theory Techn.*, vol. 60, no. 7, pp. 2142–2151, Jul. 2012.

[33] J. Song, X. Li, and H. Zhu, "A 16-bit chipless RFID tag with quasi-complementary structure," in *Proc. 6th Asia–Pacific Conf. Antennas Propag. (APCAP)*, Oct. 2017, pp. 1–3.

[34] M. A. Ashraf, Y. A. Alshoudokhi, H. M. Behairy, M. R. Alshareef, S. A. Alshebeili, K. Issa, and H. Fathallah, "Design and analysis of multi-resonators loaded broadband antipodal tapered slot antenna for chipless RFID applications," *IEEE Access*, vol. 5, pp. 25798–25807, 2017.

[35] Y. F. Weng, S. W. Cheung, T. I. Yuk, and L. Liu, "Design of chipless UWB RFID system using a CPW multi-resonator," *IEEE Antennas Propag. Mag.*, vol. 55, no. 1, pp. 13–31, Feb. 2013.

[36] C. M. Nijas, R. Dinesh, U. Deepak, A. Rasheed, S. Mridula, K. Vasudevan, and P. Mohanan, "Chipless RFID tag using multiple microstrip open stub resonators," *IEEE Trans. Antennas Propag.*, vol. 60, no. 9, pp. 4429–4432, Sep. 2012.

MOHD EZWAN B JALIL received the degree in electrical engineering -telecommunication from the Universiti Teknologi Malaysia, in 2010, the master's degree in electrical engineering, in 2013, and the Ph.D. degree in electrical engineering, in 2014. He also did his internship at Rennes University, in 2014, under the supervision of Prof. Dr Himdi. His research interests include wearable antennas, chipless RFID, and metamaterials. He has published numerous journals, such as *Applied Physic*, *Progress in Electromagnetic Research*, proceedings, such as International Symposium on Antennas and Propagation (ISAP) and European Conference on Antennas and Propagation. He received several universities and national awards related to his research works; wearable antenna. He has been appointed as a Reviewer for several national/international journals, such as IEEE Access. He is also an Active Researcher in Advanced RF and Antenna Research Group (ARFMRG) and has been participating in a lot of courses, seminars, exhibition, and so on.

MOHAMAD KAMAL A RAHIM (Senior Member, IEEE) received the B Eng. degree in electrical and electronic engineering from the University of Strathclyde, U.K., in 1987, the M.Eng. degree in science from the University of New South Wales, Australia, in 1992, and the Ph.D. degree in electrical engineering from the University of Birmingham, U.K., in 2003. From 1987 to 1989, he worked as a Management Trainee with Sime Tyres Mergong Alor Star Kedah and a Production Supervisor with Sime Shoes, Kulim Kedah. He joined the Department of Communication Engineering, Faculty of Electrical Engineering, Universiti Teknologi Malaysia, Kuala Lumpur, as an Assistant Lecturer, in 1989. He was appointed as a Lecturer with the Faculty of Electrical Engineering. He was appointed as a Senior Lecturer, in 2005. He was appointed as an Associate Professor with the Faculty, in 2007. He is currently a Professor of RF and antenna with the Faculty of Electrical Engineering, Universiti Teknologi Malaysia. He has published over 200 articles in journals and conference papers. His research interests include design of dielectric resonator antennas, microstrip antennas, small antennas, microwave sensors, RFID antennas for readers and tags, multi-function antennas, microwave circuits, EBG, artificial magnetic conductors, metamaterials, phased array antennas, computer-aided design for antennas, and design of millimeter frequency antennas.

HIMDI MOHAMED received the Ph.D. degree in signal processing and telecommunications from the University of Rennes 1, France, in 1990. Since 2003, he has been a Professor with the University of Rennes 1, and the Head of the High Frequency and Antenna Department, IETR, in 2013. He has authored or coauthored 141 journal articles and over 280 papers in conference proceedings. He has also coauthored nine book chapters. He holds 46 patents. His research interests include passive and active millimeter-wave antennas, development of new architectures of antenna arrays, and new three-dimensional (3-D) antenna technologies. He was a Laureate of the 2d National Competition for the Creation of Enterprises in Innovative Technologies, in 2000, (Ministry of Industry and Education). He received the JEC-AWARD at Paris on Pure composite material antenna embedded into a motorhome roof for the Digital Terrestrial Television reception, in March 2015.

NOOR ASMAWATI BINTI SAMSURI (Member, IEEE) was born in March 1980. She received the B.S. degree in electrical engineering (telecommunication) from the Universiti Teknologi Malaysia, Johor, in 2001, and the M.Sc. degree in digital communication systems and the Ph.D. degree in electronic and electrical engineering from Loughborough University, U.K., in 2004 and 2009, respectively. Her current research interests include an antenna for the mobile handset, antenna interaction and coupling with human and metallic jewelry, and EM field absorption (SAR). Her awards and honors include the Frew Fellowship (Australian Academy of Science), the I. I. Rabi Prize (APS), the European Frequency and Time Forum Award, the Carl Zeiss Research Award, the William F. Meggers Award, and the Adolph Lomb Medal (OSA).

NOOR ASNIZA MURAD (Senior Member, IEEE) received the first degree in electrical engineering majoring in telecommunication and the master's degree in engineering from the Universiti Teknologi Malaysia (UTM), in 2001 and 2003, respectively, and the Ph.D. degree, in 2011, for research on micromachined millimeterwave circuits under supervision of Professor Lancaster. She joined the Department of Radio Communication Engineering (RaCED), Faculty of Electrical Engineering (FKE), UTM, as a Tutor. She has been appointed as a Lecturer, in April 2003. She joined the Emerging Device Technology Group, University of Birmingham, U.K. She was with HID GLOBAL Sdn Bhd for one year under Research and Development specifically working on RFID tag design, testing and development. She is leading the Advance RF and Microwave Research Group, School of Electrical Engineering, UTM. Her research interests include antenna design for RF and microwave communication systems, millimeter-wave circuits design, RFID, and antenna beamforming. She is a member of Antenna and Propagation (AP/MTT/EMC) Malaysia Chapter.

RAIMI DEWAN (Member, IEEE) received the bachelor's degree in electrical and telecommunication engineering, and the master's and Ph.D. degrees in electrical engineering from the Universiti Teknologi Malaysia (UTM), in 2010, 2013, and 2019, respectively. Prior joining UTM, he was a UHF RFID Product Coordinator with HID Global. From 2019 to 2020, he joined the Institute of Electronics and Telecommunications of Rennes, University of Rennes 1, France as a Postdoctoral Researcher. As a Postdoctoral Researcher, he is actively working with Naval Group and Seribase for the projects under the Ministry of Arms (DGA) France. He was a Senior Materials Engineer with Keysight Technologies, in 2018. He is currently a Senior Lecturer with the School of Biomedical Engineering and Health Science, UTM. His research interests include RF and microwave field. He also serves as the active Reviewer for various International journals, including IEEE Access, the IEEE Microwave and Wireless Components Letters, *PIER*, the *International Journal of Electronics and Communications*, *Renewable and Sustainable Energy Reviews*, *WPC*, *IET Electronic Letters*, *IET MAP*, and the *International Journal of RF and Microwave Computer-Aided Engineering*.

HUDA BIN A MAJID (Member, IEEE) received the Ph.D. degree in electrical engineering from the Universiti Teknologi Malaysia (UTM). He worked as a Postdoctoral Fellow with UTM for a period of one year. He is currently a Lecturer with the Faculty Engineering Technology, Universiti Tun Hussein Onn Malaysia (UTHM), Batu Pahat, Johor. He has published over 100 articles in journals and conference papers. His research interests include planar and flexible antennas, array antennas, reconfigurable antennas, metamaterial, and RF microwave and mm-wave devices.

LEVY OLIVIA NUR (Member, IEEE) received the B.E., M.E., and D.E. degrees in electrical engineering, majoring in telecommunication engineering from the Institut Teknologi Bandung, Indonesia, in 2001, 2004, and 2014, respectively. From 2002 to 2003, during her study in master's program she joined the Japanese University Studies in Science Technology (JUSST), University of ElectroCommunications (UEC), Tokyo, Japan. Since 2010, she has been a Lecturer with Telkom University (previously known as Institut Teknologi Telkom, ITTelkom), Bandung, Indonesia. Her research interests include microwave absorbent material, wearable antenna, and its characterization.

BAMBANG SETIA NUGROHO (Member, IEEE) graduated from the Department of Electrical Engineering (majoring Telecommunications), Institut Teknologi Bandung (ITB), Bandung, Indonesia, in 1999. He received the master's degree from the Graduate School of Electrical Engineering, ITB, in 2004, and the Ph.D. degree from the Graduate School of Electrical Engineering, Universitas Indonesia, in 2015. Since 1999, he has been working as a Lecturer and a Researcher with the School of Electrical Engineering, Telkom University, Indonesia. He has authored around 25 scientific publications in this area. His research interests include microwave technology, antenna engineering, and electromagnetics. He is also a member of the Antenna and Propagation Society and Communication Society. He was involved as a Reviewer of the International conference in telecommunications, and also active in conducting research in the field of antenna engineering, microwave devices and wearable electromagnetic wave absorbing materials.

NUR BIHA MOHAMED NAFIS received the bachelor's degree in instrumentation science and the master's degree in applied physics from the Universiti Putra Malaysia (UPM). She is currently pursuing the Ph.D. degree in electrical engineering with the Universiti Teknologi Malaysia (UTM).

. . .